JOURNAL OF MATERIALS SCIENCE 15 (1980) 1915–1925

The structure of plasma-prepared Al_2O_3–TiO_2 powders

M. S. J. GANI, R. McPHERSON
Department of Materials Engineering, Monash University, Clayton, 3168, Victoria, Australia

The morphology and phase constitution of sub-micron Al_2O_3–TiO_2 powders prepared by oxidation of mixtures of Al_2Br_6 and $TiCl_4$ in an oxygen–argon high-frequency plasma have been studied. The particle size and distribution were consistent with formation of liquid particles by rapid nucleation and surface reaction followed by growth by coalescence of droplets. The particle size of the powders is related to the concentration of reactants in the gas stream and the temperature difference between condensation and solidification. A metastable solution of TiO_2 in δ-Al_2O_3 was formed in the range 0 to 7 wt% TiO_2, at higher TiO_2 concentrations particles consisted of a dispersion of rutile particles (~ 10 nm) within single crystals of δ-Al_2O_3. A metastable phase identified as $3Al_2O_3 \cdot TiO_2$ was also formed in powder with compositions in the range 14 to 40 wt% TiO_2. Over the composition range 40 to 80 wt% TiO_2 the powder consisted predominantly of crystals with a two-phase Al_2TiO_5–rutile structure. Pure TiO_2 consisted largely of anatase and the addition of Al_2O_3 resulted in the formation of rutile as the major phase. The phase constitution of the powders is interpreted in terms of the nucleation kinetics of the various phases.

1. Introduction

Sub-micron powders of refractory compounds may be prepared by a variety of high-temperature techniques, usually involving the reaction between a volatile compound and gas in a combustion flame [1], d.c. plasma [2] or high frequency (h.f.) plasma [3]. The h.f. plasma method has the advantage that the product is not contaminated by electrode materials and it may be used with oxygen as the plasma gas. The h.f. plasma itself tolerates only small concentrations of reactants without extinction, however, it is possible to produce oxides at a high production rate by injection of halide into the tail flame of an oxygen plasma [4]. In the case of SiO_2, Al_2O_3 and TiO_2 the reaction is completed above the melting point of the product giving a mist of liquid droplets which subsequently freeze to form metastable phases [5] as the gas stream cools. It is possible to co-condense oxides to give mixed oxide particles [6, 7] often with unusual crystal structures. The present paper discusses the structure of Al_2O_3–TiO_2 powders, co-condensed from a plasma, in terms of the processes occurring during particle formation and the changes which take place on subsequent heat treatment.

The only two equilibrium phases in the Al_2O_3–TiO_2 system, below approximately 1200° C, are α-Al_2O_3 and rutile [8]. The solid solubility of TiO_2 in α-Al_2O_3 is reported to be approximately 0.20 wt% at 1300° C [9] and 1.97 wt% α-Al_2O_3 in rutile at 1426° C [10]. Aluminium titanate Al_2TiO_5 is the only stable compound, two crystalline forms of which have been identified, α-Al_2TiO_5 stable only between 1820° C and the melting point, and β-Al_2TiO_5 at lower temperatures [8]. There is some doubt concerning the lower limit of stability of Al_2TiO_5; Lang *et al.* [8] reported that it decomposed to α-Al_2O_3 and rutile between 750 and 1300° C and Hamelin [11] observed no reaction between the oxides at 1250° C but complete reaction at 1450° C. A tem-

0022–2461/80/081915–11$03.10/0

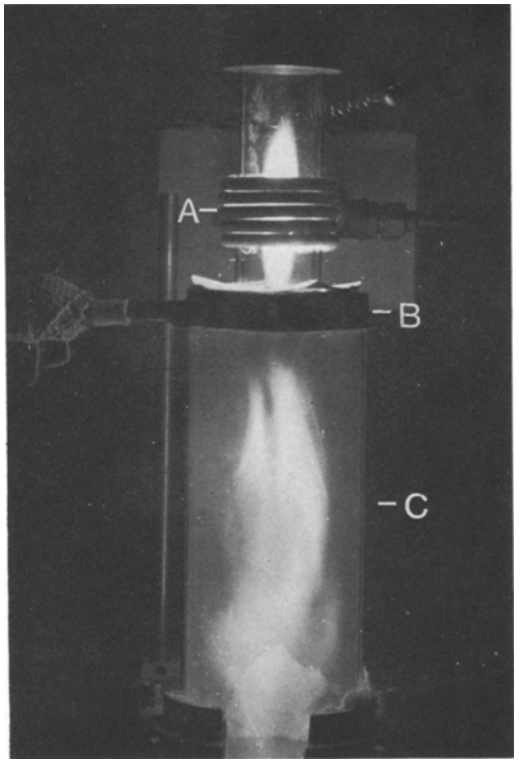

Figure 1 Plasma reactor in operation. A, plasma torch; B, injection manifold for halides; C, Pyrex reaction tube.

perature of formation of Al_2TiO_5, determined by DTA, of 1380° C was reported by Bhattacharyya and Sen [12], however, Imlach and Glasser [13] reported that the reaction occurred reversibly at 1262 ± 7° C. It has been reported that the rate of decomposition of Al_2TiO_5 is dependent upon purity [8] and Goldberg [14], who gave 1200° C as the lower limit of stability of pure Al_2TiO_5, observed that it was stabilized to room temperature by addition of Fe_2O_3.

2. Experimental details

The apparatus used for powder preparation has been described in detail elsewhere [15]. Briefly it was based on a high-frequency torch consisting of a 43 mm outside diameter (o.d.) silica tube surrounded by a coil supplied with current at 5 MHz at powers up to 15 kW. The torch tube was cooled by a flow of oxygen within the 1.5 mm annular gap between it and a surrounding silica tube 49 mm o.d. The torch was stabilized by helical flow of the plasma gas. The usual operating conditions were: 10 litre min^{-1} Ar, 20 litre min^{-1} O_2 plasma gas and 10 litre min^{-1} O_2 cooling gas, at a power input of approximately 10 kW. Mixed halides, in argon as the carrier gas, were injected into the gas stream just below the plasma through four radial holes in an annular stainless steel manifold surrounding the lower part of the plasma. Reaction between the halides and plasma gas took place in a pyrex tube, 100 mm diameter and 700 mm long, below the manifold as illustrated in Fig. 1. The powder product was collected by passing the gas stream through an electrostatic precipitator operating at 15 to 20 kV.

The reactants used were A.R. $TiCl_4$ and Al_2Br_6 prepared by reaction between A.R. bromine and 99.99% aluminium foil [16]. Introduction of the reactants into the plasma in controlled proportions was achieved by bubbling argon consecutively through $TiCl_4$ and Al_2Br_6 held at constant temperatures in Pyrex flasks. The temperatures of the reactants were controlled from thermocouples within glass sheaths in the flasks using electronic temperature control of electric heating mantles around the flasks. Electrically heated glass tubes were used between the manifold and reactant flasks to prevent condensation of the halides. The rate of powder production was varied between 1 and 15 g min^{-1} by control of the flow rate of argon through the reactants and their temperature. Some experiments were also conducted in which oxygen was injected into the reaction zone, at a rate of 100 litre min^{-1}, by an additional manifold containing a number of radial holes situated 90 mm below the reactant inlet.

The particle-size distribution of the powders was determined by measuring their diameters on electron micrographs. A sample of powder was dispersed ultrasonically in an alcohol–water mixture and a drop of the suspension allowed to evaporate on a carbon film on a copper microscope grid. The particle diameter and frequency were measured on prints of the electron micrographs, at a magnification of × 56000 or × 90000, using a Zeiss TG23 particle size analyser. The results were plotted as a cumulative size distribution on log probability paper and the geometric means and standards deviations read directly from the plot (all distributions were log normal). Between 1000 and 3000 particles were counted for each powder sample to obtain a reliable distribution curve [17].

Powder compositions were determined by a commercial analyst using sodium metaborate fusion followed by atomic absorption spectrometry. Analysis of individual particles within three of the powders (19.8, 44,2 and 78.3 wt % TiO_2)

was carried out by G. Lorimer, University of Manchester, using an analytical electron microscope (EMMA-4) equipped with wavelength dispersive spectrometers [18].

The phases present in the powders, in the as-prepared condition and after heat treatment, were determined by X-ray diffraction using a Philips diffractometer. The patterns of many of the powders were extremely complex and consisted of numerous broad and often overlapping lines. Interpretation of these patterns was simplified by the use of step scanning, at 0.5° 2θ intervals, with 40 sec count time per step.

Phase transformations occurring during heating of as-prepared samples were also investigated by differential thermal analysis using a Rigaku high-temperature micro DTA apparatus at a heating rate of 20° C min^{-1} up to 1500° C. The transformations occurring at DTA peaks were determined by X-ray diffraction of samples just before and after the peak temperature.

The structure of individual powder particles was examined by transmission electron microscopy using a JEOL 100 C microscope. The spherical powder particles were usually transparent and it was difficult in some cases to determine whether features of the structure were on the particle surface or in the interior. Particle sections of these powders were therefore prepared by ion beam thinning of thin slices prepared from isostatically pressed compacts by grinding and polishing [19].

3. Results

A number of powders were prepared over the composition range from pure Al_2O_3 to pure TiO_2. Their compositions, particle size and standard deviation, production rate and phases present are given in Table I.

3.1. Phases present in as-prepared powders

3.1.1. 0 to 7 wt % TiO_2

The X-ray diffraction pattern for pure Al_2O_3 powders corresponded very closely with that given by Rooksby and Rooymans [20] for δ-Al_2O_3 prepared by decomposition of boehmite. A few additional weak lines were also detected which did not correspond with lines of any of the other forms of alumina.

Transmission electron microscopy showed that the pure Al_2O_3 powder consisted of spherical particles, each consisting of a single crystal, many of which showed contrast from planar defects (Fig. 2). The electron diffraction patterns were quite complex with numerous super lattice spots and some streaking as previously reported by Lippens and de Boer for δ-Al_2O_3 [21].

The morphology of all powders containing up to 7.4 wt % TiO_2 was similar to that for pure alumina, the only differences detected were slight changes in the intensity of some of the X-ray diffraction peaks, and the presence of more defects within the particles revealed by contrast in the electron micrographs (Fig. 3).

3.1.2. 14 to 39 wt % TiO_2

In this composition range, X-ray diffraction showed the presence of δ-Al_2O_3, rutile and a trace of α-Al_2O_3, in addition to some intense lines which did not correspond to those of any known phase in the Al_2O_3–TiO_2 system.

The lines which remained after subtracting those for δ-Al_2O_3, rutile and α-Al_2O_3 are given in Table II and were assumed to originate from a previously unknown "phase-X".

Electron micrographs of particles in this composition range showed the presence of particles with two distinct morphologies. The majority were spherical with a spotted appearance suggesting a two-phase structure (Fig. 4). Identification was difficult because the selected-area diffraction patterns were strongly streaked; however, in a few cases indexation of the single-crystal pattern as δ-Al_2O_3 was possible. Particles were then tilted under dark-field conditions until one or more of the second-phase particles were illuminated. The patterns obtained for these conditions agreed with that of rutile and dark-field examination revealed that the rutile particles were randomly oriented with respect to the δ-Al_2O_3 matrix. The irregular outline of the spheres suggested that perhaps the rutile particles were located on the surface; however, transmission electron micrographs of ion-thinned sections showed that the rutile was distributed within the spheres of δ-Al_2O_3 as particles approximately 10 nm in size (Fig. 5).

The other particle type present was non-spherical (Fig. 6a) and shadowing with gold showed that they were approximately equi-axed rather than flat plates (Fig. 6b). Analysis of the electron diffraction pattern gave an orthorhombic structure with lattice spacings of $a = 8.3_3$, $b = 8.6_2$ and $c = 9.4_7$ Å. Calculated d-spacings using this unit cell gave reasonable agreement with the

TABLE I Powder composition, particle size, standard deviation of particle size, production rate and phases present

No.	TiO2 (wt%)	Mean particle diameter of log-normal distribution (nm)	Standard deviation particle diameter (log σ)	Powder production rate ($g\,min^{-1}$)	Phases present
1	0	40	0.128	5	
2	0	38	0.159	1	
3	0	92	0.214	10	
4	1.6	119	0.202	5	
5	3.4	36	0.172	1	
6	5.0	61	0.151	1	δ-Al_2O_3
7	5.3*	37	0.105	1	
8	6.4	43	0.144	0.5	
9	7.4	135	0.249	8	
10	14.0*	100	0.192	11	
11	14.2	140	0.173	5	
12	15.0	153	0.154	10	
13	16.4	173	0.156	6	δ-Al_2O_3,
14	19.8	131	0.170	11	phase-X,
15	23.4	85	0.222	6	rutile
16	23.8	118	0.182	10	α-Al_2O_3
17	28.4	58	0.275	1	
18	28.7	69	0.204	1	
19	32.2	160	0.233	8	
20	34.2	134	0.164	12	δ-Al_2O_3, phase-X, rutile, α-Al_2O_3, Al_2TiO_5
21	38.6*	41	0.151	8	
22	39.7	81	0.181	4	
23	44.2	87	0.278	14	
24	47.3	124	0.177	10	Al_2TiO_5, rutile, δ-Al_2O_3
25	54.4	76	0.235	1	
26	54.5	130	0.180	8	
27	56.9	71	0.181	1	
28	61.2	135	0.168	7	
29	71.5	150	0.167	7	Al_2TiO_5, rutile
30	78.3	170	0.205	10	
31	99.0	41	0.229	2	Rutile, anatase
32	99.0	75	0.192	1	
33	100.0	46	0.246	1	Anatase, rutile

* Powders prepared with 100 litre min^{-1} oxygen injected 90 mm below reactant inlet.

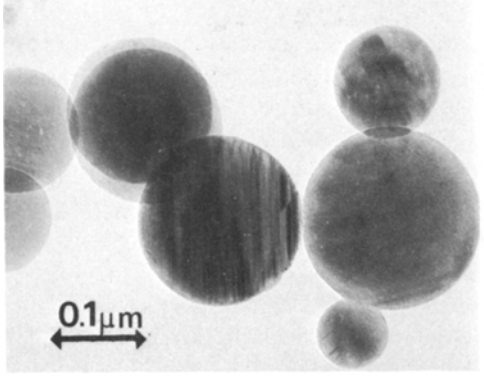

Figure 2 TEM of pure Al_2O_3 powder.

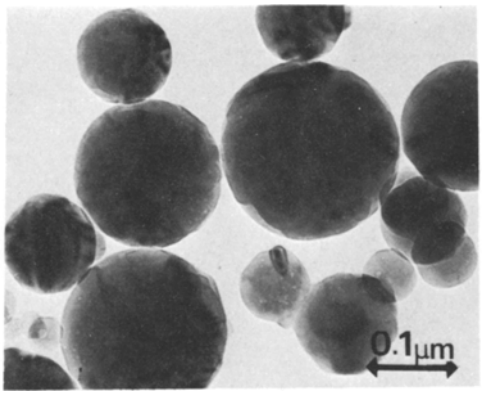

Figure 3 TEM of Al_2O_3–7.4 wt% TiO_2 powder.

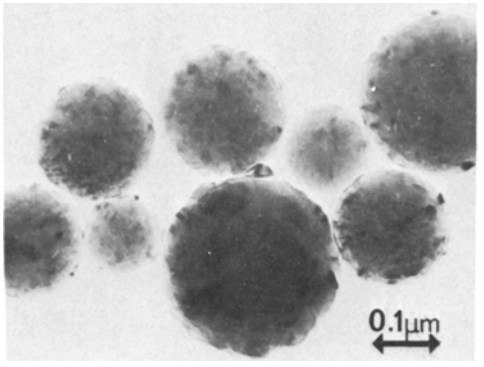

Figure 4 TEM of Al_2O_3–15 wt% TiO_2 powder.

unknown lines in the X-ray diffraction pattern confirming that the particles were "phase-X". The variation of the proportion of phase-X in the powders as a function of composition, as determined by X-ray diffraction using α-Al_2O_3 additions as an internal standard and comparing the integrated intensities of the phase-X line at 42.2° 2θ with the α-Al_2O_3 at 43.4° 2θ, showed that the maximum

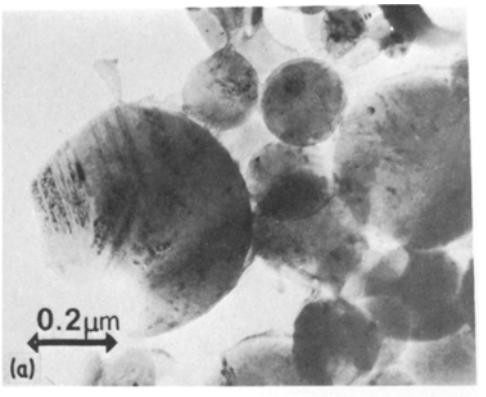

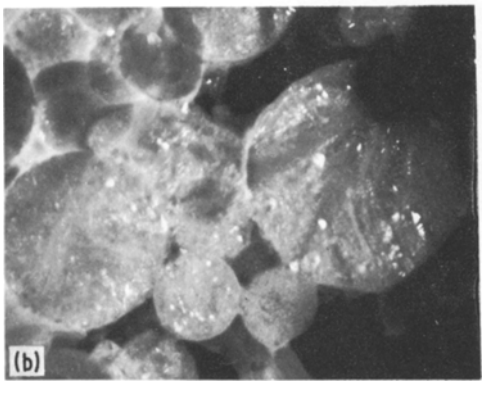

Figure 5 TEM of Al_2O_3–15 wt% TiO_2 powder compact ion-thinned. (a) Bright field; (d) dark-field using rutile diffracted beam.

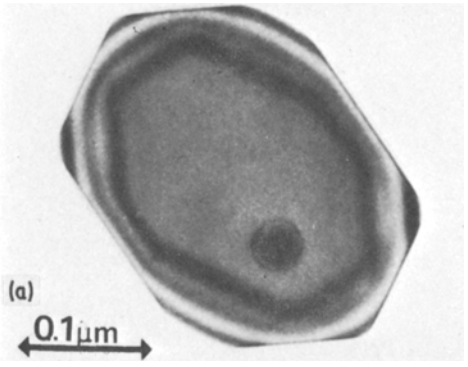

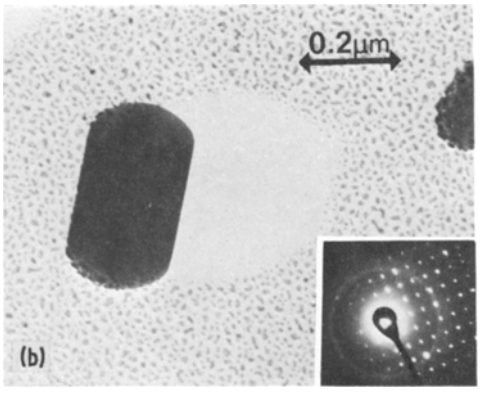

Figure 6 (a) TEM of "phase-X" particle. (b) "Phase-X" particle shadowed with gold to show its shape. Selected-area diffraction pattern.

concentration of phase-X occurred at 20 to 22 wt % TiO_2. Analysis of three of the particles by microanalysis (EMMA 4) gave values of 19.6, 22.0 and 22.1 wt % TiO_2. These figures compare closely with the composition $3Al_2O_3 \cdot TiO_2$ (20.7 wt % TiO_2) suggesting that phase-X is this compound which is metastable under all conditions.

From the volume of the unit cell and the molecular weight of phase-X, the only reasonable density is 3.77 g cm^{-3} which is similar to that of δ-Al_2O_3 and Al_2TiO_5 and therefore is in good agreement with the likely density for a phase crystallizing from Al_2O_3–TiO_2 liquid.

3.1.3. 39 to 78 wt % TiO_2

X-ray diffraction showed the phases present in these powders to be Al_2TiO_5 and rutile with some δ-Al_2O_3 (Table I). Most of the particles, were spherical in shape with complex internal structure and it was not possible to positively identify the phases present by electron diffraction (Fig. 7). The transmission electron micrographs, however, sug-

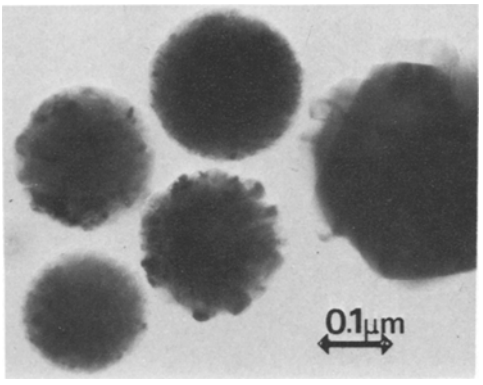

Figure 7 TEM of 54 wt % TiO_2 powder.

gested that the particles had a two-phase structure. The proportion of Al_2TiO_5 was estimated by X-ray diffraction using α-Al_2O_3 additions as an internal standard and calibration mixtures of α-Al_2O_3 and pure Al_2TiO_5; the maximum concentration of Al_2TiO_5 occurred at approximately 45 wt % TiO_2.

3.1.4. 99 to 100 wt % TiO_2

Pure TiO_2 powder consisted of a mixture of anatase and rutile with anatase as the predominant phase, however, the addition of approximately 1% Al_2O_3 resulted in a considerable decrease in the proportion of anatase, resulting in the formation of a powder consisting predominantly of rutile

3.1.5. Phase constitution as a function of composition

An approximate indication of the proportion of phases present in the powders as a function of composition, derived from the X-ray diffraction data, is presented in Fig. 8. These are based on the measured concentration of Al_2TiO_5 and the approximate concentration of phase-X, the concentrations of the other being estimated by difference.

3.2. Phase changes on heating

3.2.1. Isothermal heat treatment

The phases present in the powders after heating in

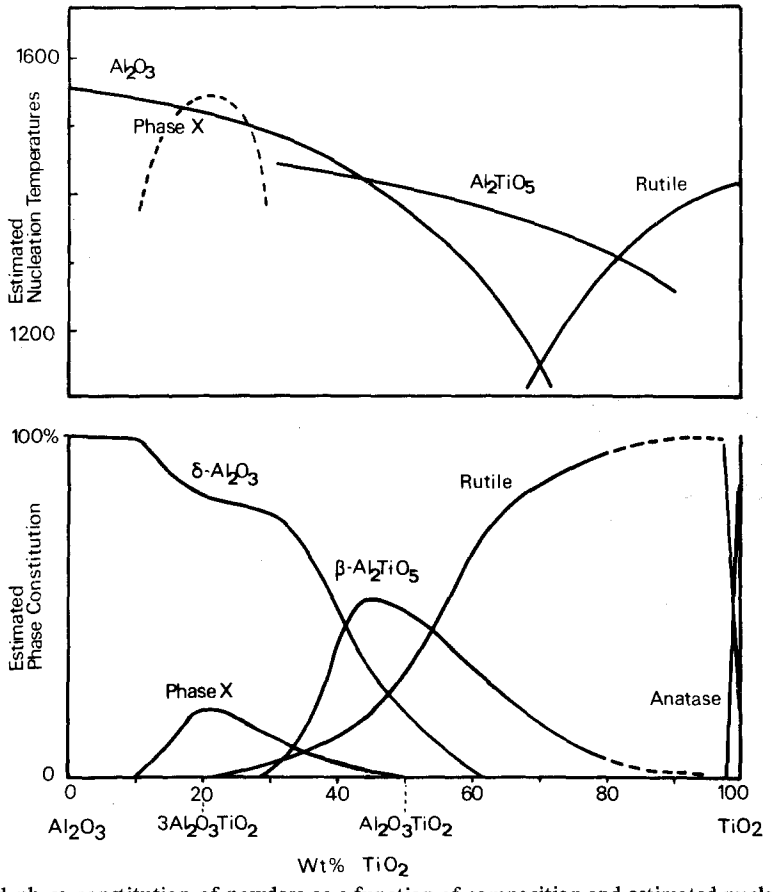

Figure 8 Estimated phase constitution of powders as a function of composition and estimated nucleation temperatures of various phases.

TABLE II X-ray diffraction d-spacings from "phase-X"

Observed d(λ)	Calculated from orthorhombic cell $a = 8.3_3$, $b = 8.6_2$, $c = 9.4_7$ Å	
	d(Å)	$h\,k\,l$
5.9	5.99	1 1 0
5.2	5.06	1 1 1
4.41	4.30	0 2 0
4.23	4.16	2 0 0
3.91	3.92	0 2 1
3.80	3.80, 3.81	1 2 0, 2 0 1
3.69	3.71	1 1 2
3.18	3.19	0 2 2
2.81	2.79	1 1 3
2.410	2.415	2 1 3
2.377	2.370	0 0 4
2.141	2.155	0 4 0
2.125	2.125, 2.120	0 3 3, 2 3 2

air at 1000, 1200 and 1400° C for 1 h, followed by rapid cooling, are given in Table III.

Heating at 1000° C resulted in dissociation of phase-X into α-Al_2O_3 and rutile and some transformation of δ-Al_2O_3 to α-$Al2O_3$ occurred in those powders containing relatively high TiO_2 contents. Transformation of δ-Al_2O_3 to α-Al_2O_3 occurred in all powders on heating to 1200° C, and rutile was formed in those powders which consisted initially of a solid solution of TiO_2 in δ-Al_2O_3. Reaction between α-Al_2O_3 and rutile to form Al_2TiO_5 occurred on heating at 1400° C in powders containing between 5 and 78 wt % TiO_2, but did not occur in powders containing less than

TABLE III Phases present after isothermal heat treatment for 1 h

TiO_2 (wt %)	1000° C	1200° C	1400° C
0	δ-Al_2O_3	δ-Al_2O_3 α-Al_2O_3	α-Al_2O_3
1.6–5.0	δ-Al_2O_3	α-Al_2O_3 Rutile	α-Al_2O_3 Rutile
5.3–7.4	δ-Al_2O_3 α-Al_2O_3	α-Al_2O_3 Rutile	α-Al_2O_3 Al_2TiO_5
14.0–23.8	δ-Al_2O_3 α-Al_2O_3 Rutile	α-Al_2O_3 Rutile	α-Al_2O_3 Al_2TiO_5
28.4–38.6	δ-Al_2O_3 α-Al_2O_3 Al_2TiO_4	α-Al_2O_3 Rutile	α-Al_2O_3 Al_2TiO_5
39.7–44.2	α-Al_2O_3 Rutile Al_2TiO_5	α-Al_2O_3 Rutile	Al_2TiO_5 Rutile
47.3–78.3	Rutile φ-Al_2O_3 δ-Al_2O_3	α-Al_2O_3 Rutile	Al_2TiO_5 Rutile
99–100	Rutile Anatase	Rutile	Rutile

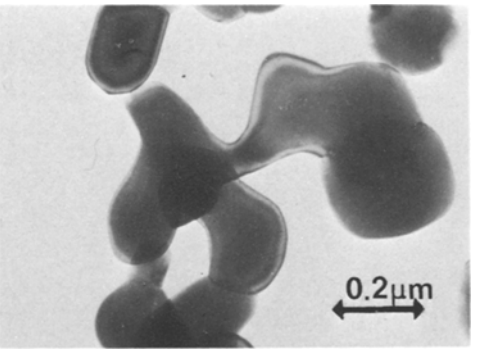

Figure 9 TEM of heat-treated 25.8 wt % TiO_2 powder showing grains of rutile and α-Al_2O_3.

5 wt % TiO_2 which remained as a mixture of α-Al_2O_3, and rutile.

Transmission electron microscopy of the heat-treated powders showed that, after heating of 1200° C, the particles had sintered together into polycrystalline arrangements in which the crystals were either rutile or α-Al_2O_3 (Fig. 9). The formation of Al_2TiO_5 at 1400° C was accompanied by considerable crystal growth with the formation of Al_2TiO_5 grains with a diameter of the order of 1 μm.

Differential thermal analysis of the powders generally gave two peaks. An exothermic reaction occurred at 1000 to 1240° C, depending on composition, which was shown by X-ray diffraction to be associated with the transformation of δ-Al_2O_3 to α-Al_2O_3 with the simultaneous formation of rutile, and an endothermic reaction at 1340 to 1450° C corresponded to the formation of Al_2TiO_5. The results are summarized in Fig. 10.

4. Discussion

4.1. Powder in formation

As discussed in a previous paper [7], liquid droplet formation in a plasma flame probably occurs by the simultaneous growth of particles by their coalescence on impact, together with reaction at the particle surfaces with the various gaseous species present in the flame. This requires partial pressures of the reactants in the flame much higher than the partial pressure of the oxide species in equilibrium with the liquid at the particle freezing point. Data for the system Al_2O_3–TiO_2 [22] shows that the vapour pressure of Al and Ti species in the plasma tail flame would be expected to be several orders of magnitude higher than the partial pressures in equilibrium with the complete range of

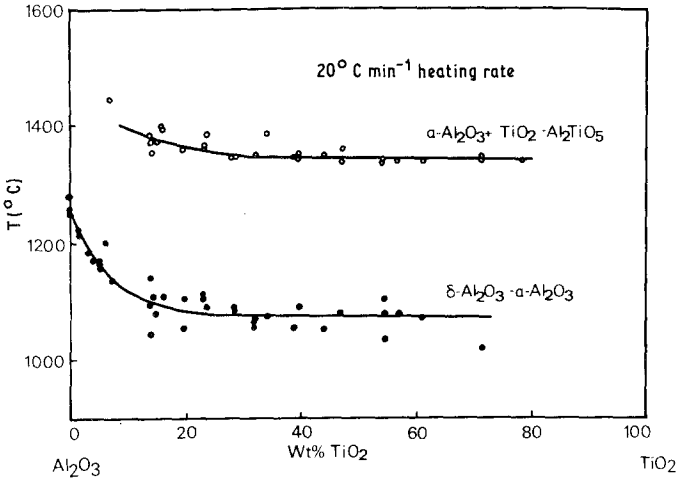

Figure 10 Variation of DTA peak temperatures with composition.

liquid solutions in the system at the liquidus temperature. It is therefore reasonable to assume that all of the powders were formed by crystallization of the droplets as they cooled in the plasma tail flame.

The particle size and distribution of the powder must also be a function of the mechanism of liquid droplet formation. Cozzi and Cadorin [23], using a mathematical model of the formation of TiO_2 particles by oxidation of $TiCl_4$ in CO–air flames, predicted that growth took place by coagulation of liquid droplets, commencing after nucleation and becoming the dominant factor when condensation and surface reaction ceased due to depletion of the reactants. Ulrich [24], assuming that the chemical reaction and nucleation times were short compared with the particle growth period by coagulation, showed that the particle-size distribution of SiO_2 powders produced by flame oxidation of $SiCl_4$ was log normal and that the particles size depended upon the time during which the particles were in the liquid state. The log normal particle-size distribution observed in the present study is therefore consistent with this model.

The ultimate particle size would be expected to depend upon the temperature range over which the particles were liquid, that is the difference between condensation and solidification temperatures and the concentration of particles, determined by the feed rate of reactants and total gas flow rate. The variation of particle size with composition and reactant concentration (powder production rate) observed in the present work is in qualitative agreement with these predictions as shown in Fig. 11 which presents the particle size for production rates of $\sim 10\,g\,min^{-1}$ and $\sim 1\,g\,min^{-1}$ together with the estimated temperatures for 99.9% condensation to liquid droplets [22], and crystallization. The latter is taken as 80% of the liquidus temperature (K) since the particles would be expected to crystallize by homogeneous nucleation [5]. It will be seen that there is an increase in particle size with increase in production rate and some evidence of increased particle size with increase in the temperature range in which the particles are liquid. Injection of cold gas into the plasma tail decreased the particle size; however, the effect is consistent simply with a dilution of the particle concentration rather than a quenching effect. The particle shape, size and size distribution therefore support a model of powder formation involving rapid liquid particle nucleation and reaction with plasma gas followed by a stage of particle growth by coagulation of liquid droplets.

This model suggests that there should be little variation in composition from particle to particle in the liquid state at the moment of crystallization. In practice there was some change in the relative reactant concentrations over the period of a production run because of the difficulty in maintaining the reactant temperature constant with the experimental arrangement used. This has therefore resulted in some variation of composition of the particles within a batch as shown by the microprobe analysis of individual particles. The variation in TiO_2 content seems not to be very large at low concentrations, as shown by the reproducibility of the transformation temperature and the uniformity in structure revealed by electron microscopy. This is not unexpected since similar change in temperature of the reactants would produce a smaller change in actual composition of the gas at low concentrations.

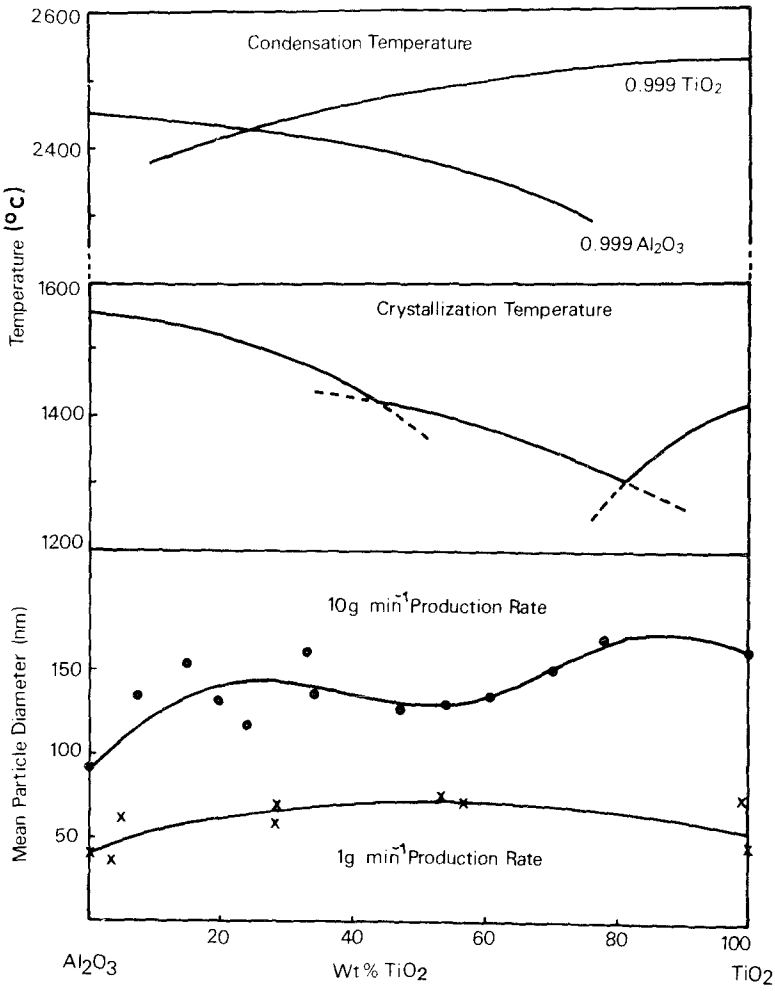

Figure 11 Mean particle diameter as a function of composition and rate of production and estimated temperature of condensation and crystallization.

4.2. Phase constitution of powder particles

The phase nucleated in a liquid droplet as it cools will depend upon the relative free energies of nucleation of all the possible crystalline phases [5]. The phase or phases actually observed in the powder will depend upon the kinetics of transformation of the nucleated phase to phases of lower free energy and the thermal history of the particles after nucleation. Thus, in certain cases, metastable phases are observed in the product, as discussed in detail for pure Al_2O_3 which probably nucleates as γ-Al_2O_3 but transforms to the more ordered δ-Al_2O_3 form during the relatively slow cooling which occurs in the tail flame of an h.f. plasma [5].

In the present study it is apparent that δ-Al_2O_3 is formed up to quite high concentrations of TiO_2. At TiO_2 levels of up to 7 wt% it is retained in solid solution in δ-Al_2O_3 but at higher concentrations duplex particles consisting of a dispersion of extremely small particles of rutile in single crystals of δ-Al_2O_3 are observed. The continued decrease of the temperature of transformation to α-Al_2O_3 at higher TiO_2 contents, however, suggests that TiO_2 is retained in solution at concentrations greater than 7 wt%.

The formation of the metastable "phase-X" ($3Al_2O_3 \cdot TiO_2$) in powders with TiO_2 contents from 14 to 38 wt% suggests that in this range, its free energy of nucleation is similar to that of γ-Al_2O_3. The fact that it was observed over a range of average powder compositions, however, may be a result of the spread in particle compositions, particularly towards the 50% TiO_2 region. The limited number of analyses of individual particles indicated a composition between 20 and 22 wt% and it is probable that $3Al_2O_3 \cdot TiO_2$ nucleated only in those particles with a composition in this

range. This is illustrated in Fig. 8 which gives estimated curves for the nucleation temperatures of the various phases in the system, (the metastable liquidus for γ-Al_2O_3 would not be very different to that for α-Al_2O_3 since the free energy difference between α-Al_2O_3 and γ-Al_2O_3 is relatively small). The nucleation curve for $3Al_2O_3 \cdot TiO_2$ is shown schematically. The observation of some α-Al_2O_3 in those powders which contain $3Al_2O_3 \cdot TiO_2$ suggests that part of the phase-X formed has later decomposed, since the heat treatment results show that it decomposes at 1000° C into α-Al_2O_3 and rutile and α-Al_2O_3 is not observed to form directly from the liquid in these powders.

The experimental results are also consistent with the nucleation of Al_2TiO_5 in the composition range of approximately 40 to 80 wt % TiO_2. It is unlikely that the Al_2TiO_5 composition range could be extended very far from stoichiometric and the observation of the peak concentration of Al_2TiO_5 near the stoichiometric value is consistent with this view. The particles with a complex structure which could not be identified (Fig. 7) are therefore probably two-phase, consisting of Al_2TiO_5 and rutile, similar in nature to the δ-Al_2O_3–rutile particles observed in the composition range 7 to 40 wt % TiO_2. The decomposition of Al_2TiO_5 at about 1100° C is within the temperature range reported by other workers [8].

As would be expected from previous studies [8, 11–13], heat treatment at 1400° C results in the formation of the equilibrium structure, either Al_2TiO_5 and α-Al_2O_3 or Al_2TiO_5 and rutile, in most of the powders. It seems surprising that Al_2TiO_5 is not detected in the powders containing less than 5 wt % heated at the same temperature, since all of the powders have a similar extremely finely disseminated structure of rutile and α-Al_2O_3. This is also reflected in the DTA data which show an increase of the reaction temperature below approximately 20 wt % TiO_2 (Fig. 10). It is difficult to accept that α-Al_2O_3 and rutile are stable in this range in view of the published data, suggesting that the effect is kinetic. The very large size of the Al_2TiO_5 crystals observed in the heat-treated powders close to the Al_2TiO_5 composition suggests that it forms from relatively few nuclei and the increase in temperature of formation at low concentrations is perhaps related to a lower probability of nucleation.

The formation of the metastable anatase form of TiO_2 rather than rutile, the only stable form, in powder prepared by high-temperature oxidation of $TiCl_4$ is well established [1, 6] and probably occurs for the same reasons that γ-Al_2O_3 and δ-Al_2O_3 form in alumina prepared by similar means [5]. The formation of rutile rather than anatase in powders containing small concentrations of Al_2O_3 is also well known and the subject of patents for pigment grade rutile manufacture [25]. The reason for the effect of Al_2O_3 is not known; the most likely explanation is probably that it influences the relative nucleation kinetics of the two forms of TiO_2 through the interfacial energy term in the classical nucleation equation. The fact that anatase and rutile are both formed in pure TiO_2 suggests that the nucleation kinetics of the two forms are similar and a relatively small change could result in the predominant formation of one phase.

5. Conclusions

The particle size, distribution and shape of mixed Al_2O_3–TiO_2 powders prepared by oxidation of $TiCl_4$ and Al_2Br_6 in an oxygen h.f. plasma flame are consistent with particle formation by rapid nucleation and reaction to form liquid droplets, followed by particle growth by coalescence until they crystallize at considerable undercooling below the equilibrium liquidus temperature.

Several metastable structures are observed in these powders; a metastable solid solution of TiO_2 in δ-Al_2O_3, a previously unreported phase $3Al_2O_3 \cdot TiO_2$ with orthorhombic structure, and anatase. The formation of these phases results from their lower free energy of nucleation from the liquid than the stable form and they are preserved to ambient temperatures because of effects associated with large undercooling, small particle size and relatively fast cooling rate.

Acknowledgements

M. S. J. Gani held a Commonwealth Post Graduate Research Award during the period in which the work was carried out. Thanks are due to G. Lorimer for electron microscope analyses of individual particles, and to Dong-Hi Lee for preparation of ion beam thinned compacts for transmission electron microscopy.

References

1. J. LONG and S. J. TEICHNER, *Rev. Int. Hautes Temp. et Réfract.* **2** (1965) 47.

2. S. F. EXELL, R. ROGGEN, J. GILLOT and B. LUX, "Fine Particles", 2nd International Conference, edited by W. E. Kuhn and E. William (Electrochemical Society, Princeton, New Jersey 1974) p. 165.
3. I. M. McKINNON and B. G. REUBEN, *J. Electrocem. Soc.* **122** (1975) 806.
4. A. AUDSLEY and R. K. BAYLISS, *J. Appl. Chem.* **19** (1969) 33.
5. R. McPHERSON, *J. Mater. Sci.* 8 (1973) 851.
6. T. I. BARRY, R. K. BAYLISS and L. A. LAY, *ibid* **3** (1968) 229.
7. M. S. J. GANI and R. McPHERSON, *ibid* **12** (1977) 999.
8. S. M. LANG, C. L. FILLIMORE and L. H. MAXWELL, *J. Res. Nat. Bur. Stand.* **48** (1952) 298.
9. E. R. WINKLER, J. F. SARVER and I. B. CUTLER, *J. Amer. Ceram. Soc.* **49** (1966) 634.
10. R. A. SLEPTYS and P. A. VAUGHAN, *J. Phys. Chem.* **73** (1969) 2157.
11. M. HAMELIN, *Bull Soc. Chim. Fr.* (1958) 1559.
12. B. N. BHATTACHARYYA and SUDHIR SEN. *Bull. Cent. Glass Ceram. Res. Int. Calcutta* **12** (1965) 92.
13. J. A. IMLACH and F. P. GLASSER, *Trans. Brit. Ceram. Soc.* **67** (1968) 581.
14. D. GOLDBERG, *Rev. Int. Hautes Temp. et Réfract.* 5 (1968) 181.
15. M. S. J. GANI and R. McPHERSON, *J. Aust. Ceram. Soc.* 8 (1972) 65.
16. D. G. NICHOLSON, P. K. WINTER and H. FINEBERG, *Inorg. Synth.* **3** (1950) 30.
17. D. W. MONTGOMERY, *Z. Werkzeit* **44** (1962).
18. G. CLIFF and G. W. LORIMER, *J. Microscop.* **103** (1975) 203.
19. D.-H. LEE and R. McPHERSON, *J. Mater. Sci.* **15** (1980) 25.
20. H. P. ROOKSBY and C. I. M. ROOYMANS, *Clay. Miner.* **4** (1961) 234.
21. B. C. LIPPENS and J. H. de BOER, *Acta. Cryst.* **17** (1964) 1312.
22. R. McPHERSON, "Proceedings of the International Round Table on Study and Application of Transport Phenomena in Thermal Plasmas", edited by C. Bonet, (I.U.P.A.C./C.N.R.S., Odeillo, 1975).
23. C. COZZI and D. CADORIN, *Combust. Sci. Technol.* **5** (1972) 213.
24. G. ULRICH, *Comb. Sci. Tech.* **4** (1971) 47.
25. E. J. MEZEY, in "Vapour Deposition", edited by C. F. Powell, J. H. Oxley and J. M. Blocher, Jr. (John Wiley and Sons, New York and London, 1966) p. 423.

Received 20 December 1978 and accepted 13 November 1979.